Cryogenics 58 (2013) 62–67

Contents lists available at ScienceDirect

Cryogenics

journal homepage: www.elsevier.com/locate/cryogenics

Electrical properties of cold-pressing welded NbTi persistent joints

Jianhua Liu *, Junsheng Cheng, Zhou Feng, Qiuliang Wang, Chang Kun, Li Xian

Institute of Electrical Engineering, Chinese Academy of Sciences, Beijing 100190, China

ARTICLE INFO

Article history:
Received 18 July 2013
Received in revised form 15 September 2013
Accepted 28 September 2013
Available online 24 October 2013

Keywords:
Persistent joints
Current decay measurement method
Cold-pressing welding
Flux creep
Magnetization relaxation

ABSTRACT

The cold-pressing welding method is employed to fabricate persistent joints between NbTi multifilamentary conductors, and a series of persistent joints are thus made at different mechanical pressures. The electrical properties of these persistent joints are tested by a joint resistance measurement device based on the current decay measurement method. Test results show that the cold-pressing welding method is reliable and applicable to NMR and MRI applications. Experiment results also shows that the joint resistances and current-carrying capacities of the joints seem to have no apparent relevance to the mechanical pressure in a wide range of 4–20 MPa, but the current decay ratio due to flux creep has obvious relevance to the mechanical pressure. Further research is needed to advance this joint manufacturing technology. Besides, measured current increase under 1 T background magnetic field is observed and explained, which has a reference meaning for testing persistent joint resistances.

© 2013 Elsevier Ltd. All rights reserved.

1. Introduction

The persistence of a magnet is vitally important for NMR and MRI applications, which is mainly dependent upon the resistive loss within the magnet system [1,2]. The resistive loss includes the resistive loss in the superconducting wires and the resistive loss in the persistent joints. The resistive loss in the superconducting wires, also known as the *n*-value losses, can be greatly reduced by increasing the current margin during the design process [3]. The resistive loss of the persistent joint can be reduced by two ways, reducing the joint resistance or/and increasing the current-carrying capacity of the persistent joints.

Multifilamentary NbTi conductors are commonly used in NMR and MRI magnets, thus persistent joints between multifilamentray NbTi conductors are very representative. Persistent joints between NbTi multifilamentary conductors can be fabricated in many ways, such as soldering [4], spot welding [5], ultrasonic welding [6], solder matrix replacement and diffusion bonding [3,7] and cold-pressing welding [8]. Cold-pressing welding technique is well employed to fabricate the persistent joints for its convenience and reliability. The NbTi/Cu wire used to make these joints is a representative NMR conductor supplied by Oxford Superconductivity Technology (OST).

There are two ways to measure the resistance of a persistent joint, the four-probe measurement method and the current decay measurement method. The four-probe measurement method has a measurement limit of $1 \times 10^{-11}\ \Omega$ [3], and is mainly employed to test the joints for high temperature superconductors. The current decay measurement method typically has a measurement sensitivity of $10^{-13}\ \Omega$–$10^{-15}\ \Omega$, and higher accuracy can be obtained by increasing the measuring time.

2. Experimental device

A joint resistance measurement system based on the current decay method is shown in Fig. 1. The fabricated joint loop is mounted onto a measurement framework, and the magnetic field generated by induced current in the joint loop can be measured by a Lakeshore low temperature Hall sensor. The background field is provided by a 3 T solenoid magnet, the axial direction of which is perpendicular to the axial directions of the Hall sensor and thus the current transformer. This kind of layout can reduce the coupling between the background magnet and the test loop to almost zero. The magnet power supply is a group of 120 A master–slave magnet power supply system. An 80 A magnet power supply is employed to power the current transformer.

Voltage taps across the Hall sensor is connected to a Keithley model 2000 Multimeter, which transfers the voltage data to a PC via an IEEE-488 buss. It takes half an hour for the measurement device to release the thermal stress after bathing in liquid helium. Nonlinear error of the Hall sensor will be compensated according to the Hall generator error plot provided by Lake Shore Cryotronics, Inc. For the current decay method, the joint resistance can be obtained from Eq. (1),

* Corresponding author. Tel.: +86 10 82547152.
E-mail addresses: liujianhua@mail.iee.ac.cn (J. Liu), qiuliang@mail.iee.ac.cn (Q. Wang).

0011-2275/$ - see front matter © 2013 Elsevier Ltd. All rights reserved.
http://dx.doi.org/10.1016/j.cryogenics.2013.09.011

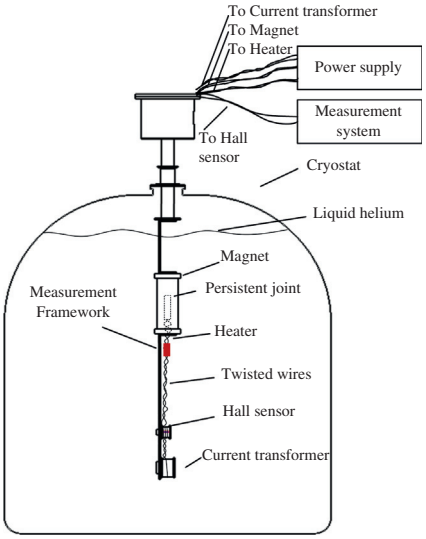

Fig. 1. Joint resistance measurement system (schematic).

$$R_j = L \cdot \frac{\ln[I_2(t_2)/I_1(t_1)]}{t_2 - t_1} \quad (1)$$

where L is the self-reluctance of the joint loop, $I_2(t_2)$ and $I_1(t_1)$ are the currents at the time t_2 and t_1, respectively.

The conservative estimate of joint resistance uncertainty from Eq. (1) is

$$\Delta R_j = L \cdot \frac{\ln[(1 + \Delta I/nI)/(1 - \Delta I/nI)]}{t_2 - t_1} \quad (2)$$

where ΔI is the current uncertainty due to the voltage scatter of the Keithley 2000 Multimeter, here is about 2.3 A, I is the induced current in the joint loop, n is the turns of the coil where the Hall sensor is placed in, typically 10.

Formula (2) shows that the measurement uncertainty can be reduced by increasing the turns of the coil or/and increasing the measuring time.

The stability level of the background field mainly depends on the stability level of the background magnet power supply, which has a stability of 0.0015%. Besides, the background magnetic field is perpendicular to the joint loop, hence the measurement error due to the uncertainty of the background magnetic field is much less than the uncertainty of the Keithley Multimeter, thus can be neglected. The maximum linear error of the Hall sensor is ±1.0% rdg, and the obtained values can further be adjusted according to the error plot provided by the Lake Shore Cryotronics, Inc.

For $\Delta I/I$ is 6×10^{-4} – 1×10^{-4} and the measuring time is about 3 h, the measurement uncertainty can be obtained from formula (2), around 2.22×10^{-14} ohm – 3.69×10^{-14} ohm.

3. Fabrication of persistent joints

The NbTi/Cu wire used to make these joints is a representative high field conductor supplied by OST, which has a bare diameter of 0.4 mm, Cu/SC ratio of 1.35 and 54 filaments. The cold-pressing welding technique includes the flowing process:

1. Remove stabilizer by nitric acid solution.
2. Rinsing the filaments by fluoric acid and pure water.
3. Cleaning the filaments by pure water and ethanol.
4. Drying the filaments in open air with air blower.
5. Braiding both filaments and installing the filament braid in CuNb tube.
6. Pressing the CuNb tube between two planar dies with a cold welding machine in open air.

Six persistent joints were made following the above process at different mechanical pressures in Step 6, and the mechanical pressure of the cold welding machine is controlled by hand. These mechanical pressures are: 1# – 4 MPa, 2# – 7 MPa, 3# – 10 MPa, 4# – 13 MPa, 5# – 16 MPa, 6# – 20 MPa. Fig. 2(a) shows the persistent joints fabricated with cold-pressing welding technology, and Fig. 2(b) shows the dimensions of the test loop, which has been illustrated in Fig. 1.

4. Experiment procedure

In order to judge the experiment more carefully, the experiment procedure has been exactly followed during the experiments. The timing diagram of the measurement system is shown in Fig. 3. The procedure includes the following steps:

1. Mount the test loop onto the experimental device as shown in Fig. 1.
2. Insert the measurement framework into the cryostat and when all the superconducting parts are immersed in the liquid helium, wait half an hour for the Hall sensor to release the thermal stress.
3. Turn on the power supply to excite the test loop at a rate of 0.2 A/s.
4. Stop exciting the current transformer at t1.
5. Turn on the heater at t2, the test loop quench at t3, and the current in the test loop decreases sharply to zero at t4.
6. Turn off the heater at t5 and wait till t6.
7. At t6, start reducing the current in the current transformer to zero at a rate of 0.2 A/s.
8. At t7, the current in the current transformer is reduced to zero, and the current in the test loop begins to decay, data used for analyzing is then collected.
9. At t8, charge the background magnet to 30 A (which generates a central magnetic field of 1 T) at 1 A/s, stop at t9.

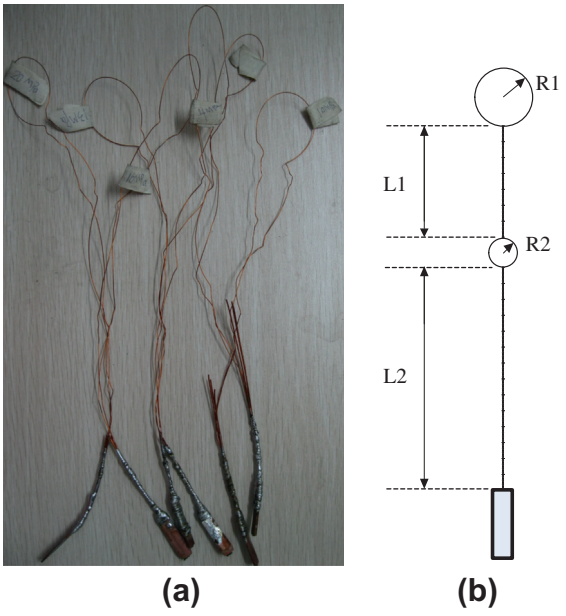

Fig. 2. Persistent joints (a) fabricated with cold-pressing welding technology, and their dimensions (b), L1 = 50 mm, L2 = 200 mm, R1 = 18 mm, R2 = 10 mm.

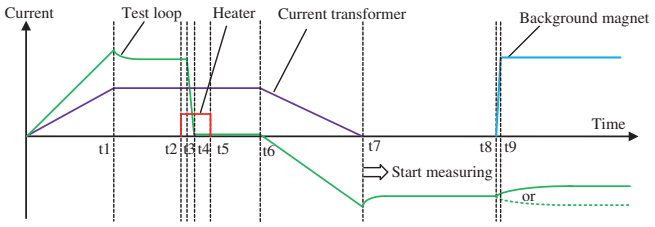

Fig. 3. Timing diagram of the measurement system (schematic).

5. Measurement results and discussion

5.1. Excitation process

Fig. 4 shows the induced currents in joint loops of 1#–6#, in a magnetic field of 0 T as a function of the excitation current of the current transformer. The maximum induced currents in the joint loop means at which the joint loop quenches or the induced current begins to decay. The joint loop cannot afford a larger induced current than the maximum induced current in the excitation process. Joint 1# – 4 MPa has the largest current-carrying capacity among these Joints, but it decayed very sharply just after the excitation process. This phenomenon happened due to the strong flux creep in this joint loop [9]. Similar phenomena were also observed when testing other joint loops, but the current decay ratio of the induced current was much smaller, and the decay amplitude was smaller either. Fig. 5 shows the current decay ratio against the mechanical pressure in the fabrication process. It can be seen that the current decay ratio is relevant to the mechanical pressure, and persistent joints made with a mechanical pressure of 10–16 MPa have much smaller flux creep effect during the excitation process. The current decay ratio is defined as:

$$\frac{\Delta I}{I_{max}} = \frac{I_{max} - I_{stable}}{I_{max}} \tag{3}$$

where I_{max} is the maximum current induced in the joint loop, I_{stable} is the current just after the sharp current decrease ends.

5.2. Flux movement in joint loops

Just after the excitation process, a sharp decrease of induced current in the joint loop has been found, as illustrated in Fig. 6. Soon after the induced current was stable, 1 T background magnetic field was exerted on the joint loop. Then we found obvious current variation in the joint loops, as illustrated in Fig. 7. Since the induced current in the joint loop is measured via the magnetic field where the Hall sensor locates, variation of magnetic field will change the "seen" current variation in the joint loop. This phenomenon can be considered as the flux movements in the persistent joints, rather than in the superconducting wire, since the induced current is much smaller than the critical current of the superconducting wire. This phenomenon can be explained by Kim–Anderson model [10,11], which gives a well-accepted analytic

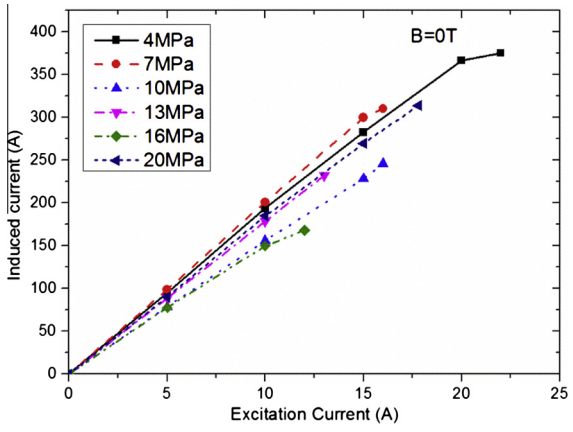

Fig. 4. The induced current in joint loops as a function of the excitation current.

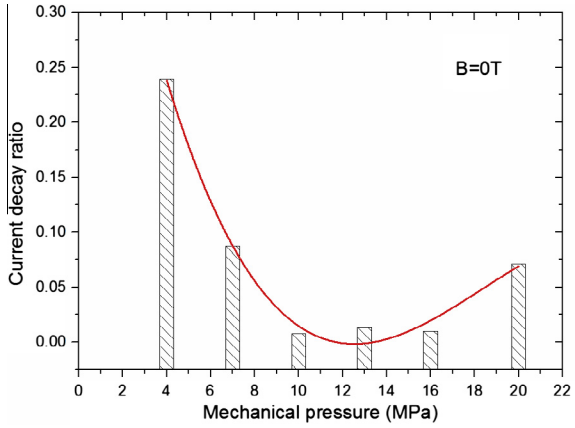

Fig. 5. Current decay ratio against mechanical pressure in the fabrication process.

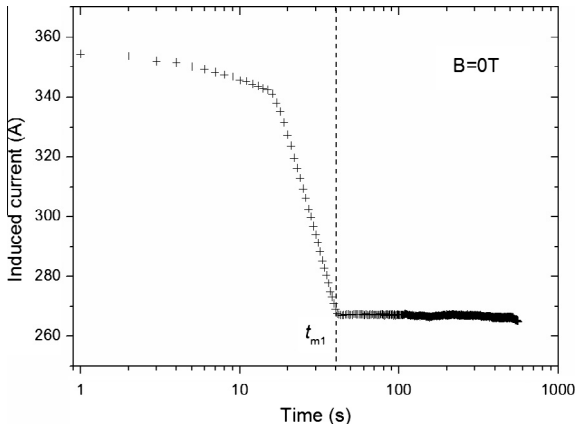

Fig. 6. Current decay in Joint 1# – 4 MPa against time under 0 T (time starts at t7 shown in Fig. 3).

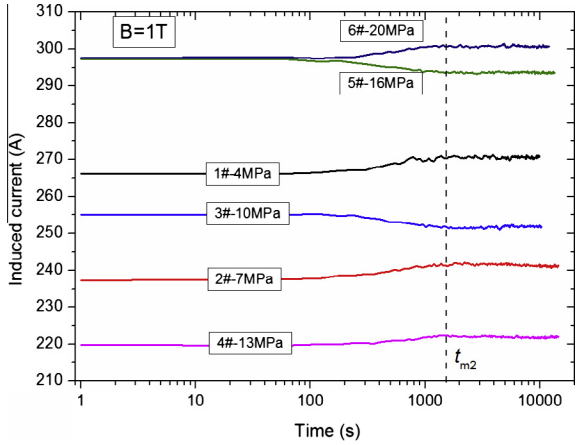

Fig. 7. Current decay against time under 1 T (time starts at t9 shown in Fig. 3).

expression for the E–J curve in the thermally-assisted flux flow (TAFF) region and flux creep (FC) region,

$$E(J) = 2\rho_c J_c \exp\left(-\frac{U_c}{\kappa_B T}\right) \sinh\left(\frac{U_c}{\kappa_B T}\cdot\frac{J}{J_c}\right) \tag{4}$$

where phenomenological parameters $J_c(B)$ is defined as the critical current density at $T = 0$, ρ_c is the resistivity at $J = J_c$, and $U(B, T)$ is the activation energy for flux jumps, κ_B is the Boltzmann constant and T is the absolute temperature.

Since the thermally-assisted flux flow has been defined as the linear part of E with respect to J, when $J \ll J_c$, (4) can be reduced to TAFF:

$$E(J) = 2\rho_c J \frac{U_c}{\kappa_B T} \exp\left(-\frac{U_c}{\kappa_B T}\right) = \rho_{\mathrm{TAFF}} J, \quad J << J_c \tag{5}$$

Then we have

$$\rho_{\mathrm{TAFF}} = 2\rho_c \frac{U_c}{\kappa_B T} \exp\left(-\frac{U_c}{\kappa_B T}\right), \quad J << J_c \tag{6}$$

Formula (6) means that ρ_{TAFF} is constant when the superconductor under a given magnetic field of B at a temperature of T. As can be seen in Fig. 6, when $t > t_{m1}$, the current $I(t)$ in the joint loop decays linearly with In(t), which corresponds with Eq. (5).

For larger current when $J \approx J_c$, (4) can be reduced to FC:

$$E(J) = \rho_c J_c \exp\left[\left(\frac{J}{J_c} - 1\right)\frac{U_c}{\kappa_B T}\right], \quad J \approx J_c \tag{7}$$

The resistivity ρ here is not a constant any more, the current $I(t)$ in the joint loop decays in a little complicated pattern, as shown in Fig. 6 when $0 < t < t_{m1}$. As the current in the joint loop decays, the persistent joint changes from the FC state into the TAFF state.

When the current in the joint loop is stable, which means the persistent joint is in the TAFF state, a 1 T background magnetic field is exerted. Slow current variation in the joint loops has been found, as shown in Fig. 7. The physical phenomenon behind this is that the flux moves slowly in the persistent joints. We define this kind of slow flux movement as magnetization relaxation. Magnetization relaxation process under 1 T background magnetic field is much slow compared to the fast thermally activated flux creep under 0 T background magnetic field.

The activation energy for flux jumps can be expressed as

$$U_c = J_c(T, B) B V_c l \tag{8}$$

where V_c the jumping volume, l is the jump width, define υ_0 as the flux creep velocity at $J = J_c$, then we have

$$B\upsilon_0 = \rho_0 J_c \tag{9}$$

Based on (8), (9), and (4) can be rewritten as

$$E(B,J) = 2\upsilon_0 B \exp\left(-\frac{B^2 V_c l \upsilon_0}{\rho_0 \kappa_B T}\right) \sinh\left(\frac{B V_c l}{\kappa_B T}\cdot J\right) \tag{10}$$

When the background magnetic field varies from 0 T to 1 T, the activation energy for flux jumps changes following (8), which will finally change the electric field in the persistent joint loop, then variation of magnetic field will occur and be seen in the form of current variation, see in Fig. 7. Magnetization relaxation in Fig. 7 may be confusing, since there are two types of magnetization relaxation, one is to increase the magnetic field where the Hall sensor locates, as 1#, 2#, 4# and 6# in Fig. 7, the other is to reduce the magnetic field where the Hall sensor locates, as 3# and 5# in Fig. 7.

This phenomenon can be explained that the flux lines in the persistent joint trapped during the excitation process relaxes during the increase of the background magnetic field. The increase of background magnetic field change the activation energy, intrinsically, the Lorentz force density $\boldsymbol{J} \times \boldsymbol{B}$ acting on the flux-line bundles increases and thus the rate of thermally activated jumps of flux-line bundles increases. The magnetic flux trapped in the persistent joint thus moves and decays, which causes the variations of the measured currents shown in Fig. 7. When exciting the persistent joint loop, quenches may happen several time during the process, as shown in Fig. 8, the final trapped magnetic fluxes in the joint loop, as indicated by j in Fig. 8, is opposite to the direction of the magnetic field generated by the induced current to be tested. Thus the decay of the trapped fluxes will increase the magnetic field where the Hall sensor locates, current increase can thus be observed, as 1#, 2#, 4# and 6# in Fig. 7. But if the final trapped magnetic fluxes is in the direction of the magnetic field generated by the current to be tested, the decay of the trapped fluxed will decrease the magnetic field where the Hall sensor locates, current increase can thus be observed, as 3# and 5# in Fig. 7.

Actually, the magnetization relaxation in Fig. 7 can also be classified into two state, the FC state when $0 < t < t_{m2}$, and the TAFF state when $t > t_{m2}$. From Figs. 6 and 7, it can be seen the FC of magnetization relaxation has a much larger time scale compared to the FC during the excitation process under 0 T background magnetic field. When testing the resistances of the persistent joints, the data should be collected when the superconductor in the TAFF state, especially the magnetization relaxation under background magnetic field should be considered so as to achieve more accurate measurements.

5.3. Joint resistances

We measured the electrical properties of all these six persistent joint loops with different mechanical pressures, and Table 1 presents the joint resistances of these joints. The joint resistances are the calculation results from Eq. (1) based on the measurement results, and time interval for the calculation is 3 h, shorter than the measurement time. The current I in Table 1 represents the stable current in the joint loop at which the resistance is measured. The

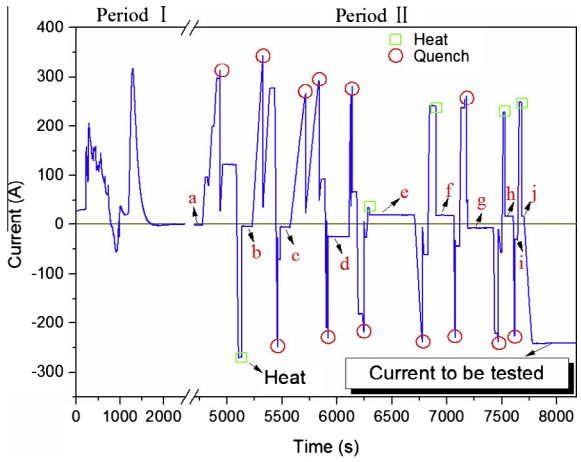

Fig. 8. Relaxation of thermal stress (Period I) and the excitation process (Period II). Thermal drift in this diagram has been compensated based on level a, the trapped fluxes as indicated by e, f, g, h, j are in the opposite direction of the magnetic field generated by the current to be tested, other trapped fluxes as indicated by b, c, d, i are in the same direction of the magnetic field generated by the current to be tested.

Table 1
Measurement results.

Joint (MPa)	R (Ω)@1 T	I (A)
1# – 4	$<1 \times 10^{-13}$	270
2# – 7	$<1 \times 10^{-13}$	240
3# – 10	$<1 \times 10^{-13}$	252
4# – 13	$<1 \times 10^{-13}$	222
5# – 16	$<1 \times 10^{-13}$	293.5
6# – 20	$<1 \times 10^{-13}$	300

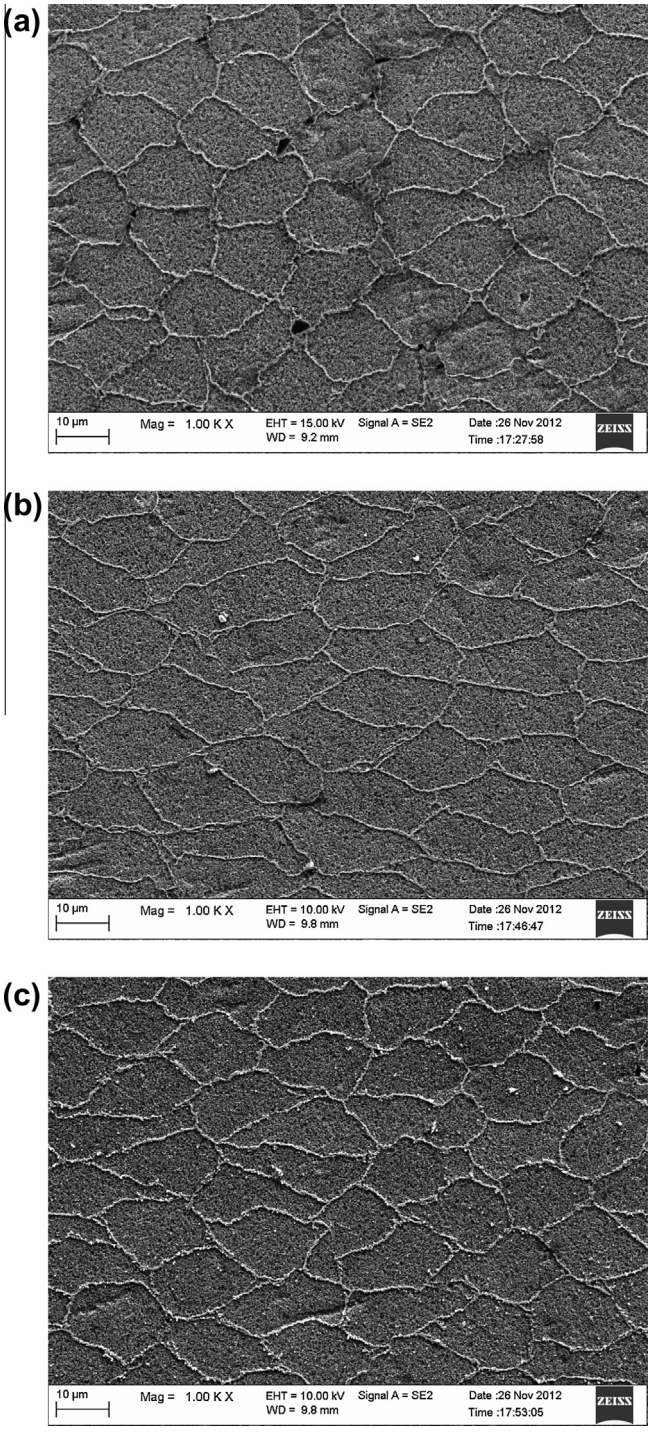

Fig. 9. Transects of persistent joints with different mechanical pressures, (a) 1# – 4 MPa, (b) 3# – 10 MPa, (c) 6# – 20 MPa.

current I can also represents the current-carrying capacity of the persistent joint, which is of key importance in NMR and MRI magnets. The persistent joint with a high current-carrying capacity can effectively reduce the training times of the magnet.

Table 1 shows that the resistances of these persistent joints are all less than 1×10^{-13} Ω in 1 T background magnetic field, and can meet the requirements of most NMR and MRI magnets. The current-carrying capacity has no apparent relevance with the mechanical pressure, but is a little higher at 16 MPa and 20 MPa, and cautious conclusion may be made based on more detailed further experimental results.

6. Microstructure of the joints

Transects of all these persistent joint were observed with scanning electron microscope (SEM), shown in Fig. 9. The microstructures of these persistent joints were a little different. The filaments in 1# persistent joint were less deformed, and obvious intervals were found in this joint, as shown in Fig. 9(a). With the increase of mechanical pressure in the fabrication process, the intervals between filaments began to disappear, as shown in Fig. 9(b), and meanwhile the filaments deformed more and more heavily, as shown in Fig. 9(c).

The untight microstructure of 1# persistent joint can explain the strong flux creep effect in the excitation process (seen in Fig. 4), but the contacts between filaments were still superconductive. Test results in Table 1 shows that the joint resistance has no apparent relevance to the mechanical pressure in a wide range from 4 MPa to 20 MPa.

7. Conclusion

Persistent joints between NbTi multifilamentary conductors fabricated using the cold-pressing welding method have low resistances and higher current-carrying capacities. A series of experiment results shows that the current-carrying capacity has no apparent relevance to the mechanical pressure, but the current decay ratio due to flux creep has obvious relevance to the mechanical pressure. Magnetization relaxation in background magnetic field has a larger time scale compared with the flux creep in the excitation process, which should be considered then testing the persistent joints. Resistances of the joints fabricated using the cold-pressing welding method are all less than 10^{-13} Ω, but the resistances of these joints has no clear relevance to the mechanical pressure in a wide range of 4–20 MPa.

Test results show that the cold-pressing welding method is very reliable and can thus be used to fabricate NbTi–NbTi multifilamentary persistent joints for NMR and MRI magnets.

Acknowledgments

This work was supported by the National Natural Science Foundation of China under Grant Nos. 50925726 and 10755001 and by the Instrument Program in MOST.

References

[1] Wang Q. High magnetic field superconducting science and technology. Beijing: Sciences Press; 2008.
[2] Wang Q. High field superconducting magnet: science, technology and applications. Progress in Physics February 2013;33(1):1–23.
[3] Swension Charles A, Denis Markiewicz W. Persistent joint development for high field NMR. IEEE Trans Appl Supercond June 1999;9(2):185–8.
[4] Seo K et al. Evaluation of solders for superconducting magnetic shield. Magn IEEE Trans 1991;27:1877–80.
[5] Phillip S et al. Two methods of fabricating reliable superconducting joints with multifilamentary Nb–Ti superconducting wire. J Low Temp Phys 1995;101:581–5.

[6] Hafstrom J et al. Joining NbTi superconductors by ultrasonic welding. IEEE Trans Magn 1977;13:94–6.
[7] Cheng Junsheng, Liu Jianhua, et al. Fabrication of NbTi superconducting joints for 400 MHz NMR application. IEEE Trans Appl Supercond 2012;22(2):4300205.
[8] Leupold MJ, Iwasa Y. Superconducting joint between multifilamentary wires 1. Joint-making and joint results. Cryogenics 1976:215–6.
[9] Tominaka T, Kakugawa S, Hara N, Maki N. Electrical properties of superconducting joint between composite conductors. IEEE Trans Appl Supercond 1991;27(2).
[10] Yamafuji K, Mawatari Y. Electromagnetic properties of high Tc superconductors: relaxation of magnetization. Cryogenics 1992;32(6):569–77.
[11] Brandt EH. The flux-line lattice in superconductors. Rep Progr Phys 1995;58(11):1465–594.